BULLETIN OF THE POLISH ACADEMY OF SCIENCES
TECHNICAL SCIENCES, Vol. 71(3), 2023, Article number: e144605
DOI: 10.24425/bpasts.2023.144605

Flywheel proof mass actuator for active vibration control

Aleksander KRAS[1]* **and Paolo GARDONIO**[2]

[1] Silencions, Bierutowska 57-59, 51-315 Wrocław, Poland
[2] DPIA, Università di Udine, Via delle Scienze 206, 33100, Udine, Italy

Abstract. This paper presents the experimental results of a new proof mass actuator for the implementation of velocity feedback control loops to reduce the flexural vibration of a thin plate structure. Classical proof mass actuators are formed by coil–magnet linear motors. These actuators can generate constant force at frequencies above the fundamental resonance frequency of the spring–magnet system, which can be used to efficiently implement point velocity feedback control loops. However, the dynamics of the spring–magnet system limit the stability and control performance of the loops when the actuators are exposed to shocks. The proof mass actuator investigated in this paper includes an additional flywheel element that improves the stability of the velocity feedback loop both by increasing the feedback gain margin and by reducing the fundamental resonance frequency of the actuator. This paper is focused on the stability and control performance of decentralized velocity feedback control loops.

Key words: inerter; proof mass actuator; velocity feedback.

1. INTRODUCTION

This paper presents an experimental study on a new proof mass actuator with a flywheel element, for active vibration control in a velocity feedback control loop to reduce flexural vibration of a thin panel. A stability and performance study is presented to assess how the additional flywheel element improves the overall control performance of the velocity feedback loop compared to the classical configurations of the actuator.

Feedback control with a collocated actuator and velocity sensor can be used to generate an active vibration control system to reduce flexural vibrations of thin plate structures [1–10].
In practice, a localized control point force is generated with proof mass actuators [11, 12]. Typically, a classical proof mass actuator is built with an outer cylindrical coil winding suspended with soft springs to an inner cylindrical magnet [13]. The pair of forces are produced by the actuator when current flows through the coil, such that one force is produced at its base and a reactive force is balanced by the inertial effect of the suspended coil [14]. The produced force is constant only at frequencies above the fundamental resonance frequency of the actuator. Thus, this actuator can be effectively used to implement an actuator-sensor velocity feedback control loop at frequencies greater than its fundamental resonance frequency [9–12]. An ideal proof mass actuator for the velocity feedback control requires low fundamental resonance frequency, which can be achieved with a comparatively soft suspension spring and heavy proof mass, which in practical use causes instability of feedback control loops when exposed to shocks or sudden accelerations [15, 16]. Thus, the effectiveness of the velocity feedback loop using a classical proof mass actuator is limited by stability issues caused by the low-frequency dynamics of the actuator [5, 7, 8].

Several different solutions and designs were proposed to overcome the limitations of low-frequency dynamics of proof mass actuators. Blended, displacement, or force feedback control was proposed for more robust active vibration control using proof mass actuators [17–19]. A compensation filter was proposed, which shifts the fundamental resonant frequency of the actuator to lower frequencies without increasing its proof mass weight [20]. Another proposed solution was
nonlinear control of the actuator to reduce the excessive oscillations of the proof mass to prevent the actuator from hitting its stop ends and thus causing instability of the feedback loops [21]. Nevertheless, the proposed solutions add complexity to the vibration control unit, and thus increase integration difficulty and operating costs of the control system.

The mechanical element called “inerter” [22], which is widely investigated in the literature [23,24], shows an enormous potential. However, the proposed solutions present idealized mechanisms that neglect the kinematic backlash and dynamic stiffness in the gearing mechanisms that convert small axial oscillations into angular oscillations of the flywheels [25, 26]. Similar studies present theoretical analysis [24], whereas this manuscript focuses only on practical aspects of the new type of actuator and presents experimental test results with a comparison to classical, off-the-shelf transducers.

The actuator investigated in this paper is based on a classical proof mass actuator design with an additional flywheel element attached to the coil armature that increases the inertia effect of the proof mass. The new actuator design aims to improve the robustness and performance of the velocity feedback control

*e-mail: aleksander.kras@gmail.com

Manuscript submitted 2022-09-30, revised 2023-01-19, initially accepted for publication 2023-02-07, published in June 2023.

loops by increasing the inertance of the actuator, which reduces fundamental resonance frequency without increasing the total weight of the actuator.

This paper is organized into five parts. Section 2 describes the three proof mass actuators compared in this study. The classical proof mass actuator, presented as a reference system, same mass as the flywheel configuration actuator and flywheel proof mass actuator. Section 3 presents the stability analysis, while Section 4 the control performance of the active vibration control. Conclusions are discussed in the concluding section.

2. FLYWHEEL PROOF MASS ACTUATOR

The proof mass actuator shown in Fig. 1, is an electromagnetic transducer, which transforms electrical energy to mechanical point force. The classical configuration presented in Fig. 1a is formed by an inner cylindrical permanent magnet which is connected, via flexure springs, to an external ferromagnetic armature where a coil is housed. The sketch on the left-hand side shows the lumped electro-mechanical parameter model of the proof mass actuator. The masses indicated with M_a and m_b represent the external ferromagnetic cylindrical element with a coil and a permanent magnet, respectively. The soft flexure springs are modeled with spring k_a and dashpot c_a. The electrical effects are modeled in terms of inherent resistance R_e, inductance L_e and electromagnetic transduction coefficient ψ. When voltage u_a is applied at the electrical terminals of the transducer and current i_a flows through the coil, pair forces F_a are generated. One force acts at the base, where the actuator is attached and a reactive force acts at the proof mass, which is external coil armature.

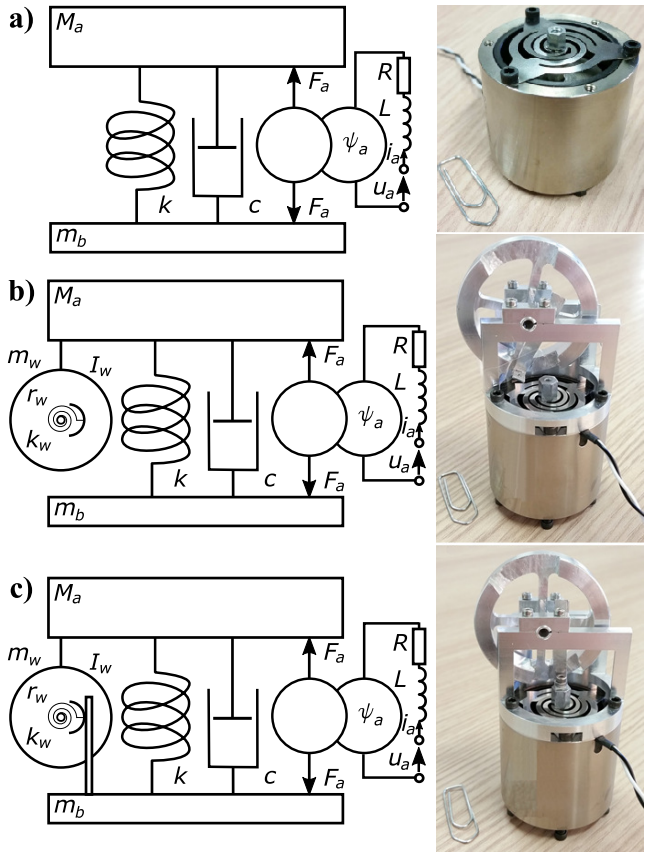

Fig. 1. Sketches (left-hand side) and pictures (right-hand side) of the classical proof mass actuator, same proof mass as the flywheel configuration (b) and flywheel proof mass actuator (c)

The second prototype considered in this study shown in the sketch and picture of Fig. 1b is the classical configuration with the same proof mass as that of the flywheel configuration. In this configuration the proof mass M_a of the classical configuration is increased by the additional mass of the flywheel element m_w and its supporting bracket, which is attached to the coil armature. However, the pin linking the flywheel element with the base mass is disengaged and no inertia effect is created when there are small oscillatory movements between the proof and base mass of the transducer.

The final configuration shown in the sketch and picture of Fig. 1c is the flywheel proof mass actuator. In this configuration, the pin linking the flywheel element and base mass to engaged means that small linear oscillations between proof and base mass are transformed into small rotational oscillations of the flywheel element and thus additional inertance is included in the mechanical properties of the proof mass actuator. The physical parameters of the proof mass actuators considered in this study are reported in Table 1.

Table 1
Mechanical parameters of the proof mass actuators

Parameter	Value
Proof mass	$M_a = 0.185$ kg
Flywheel mass	$m_w = 0.045$ kg
Base mass	$m_b = 0.115$ kg
Axial stiffness	$k = 2950$ Nm^{-1}
Torsional stiffness	$k_w = 0.009$ Nmrad^{-1}
Damping ratio	$\zeta = 0.2$
Flywheel inertia	$I_w = 42 \times 10^{-6}$ kgm^2
Flywheel offset radius	$r_w = 0.011$ m
Flywheel inertance	$I_w/r_w^2 = 0.353$ kg
Transduction coefficient	$\psi_a = 22.5$ NA^{-1}
Coil resistance	$R = 22.5\ \Omega$
Coil inductance	$L = 4.35 \times 10^{-3}$ H

3. STABILITY

This section assesses the stability of the tested velocity feedback loops implemented on thin rectangular plates using the classical with the same proof mass as the flywheel configuration and flywheel proof mass actuators. The experimental results carried out on a plate were confronted in reference to the open loop velocity sensor-actuator frequency response functions for the voltage-driven proof mass actuators. The stability

of the velocity feedback loops was assessed using the Nyquist criterion [5, 8].

Figure 2 shows the Bode plot while Fig. 3 shows the Nyquist plot. Both figures show the open loop sensor actuator frequency response functions considering the plate equipped with a classical proof mass actuator (solid black line), with the classical configuration with the same proof mass as that of the flywheel configuration (blue dashed line) and with the flywheel proof mass actuator (red dash-dotted line).

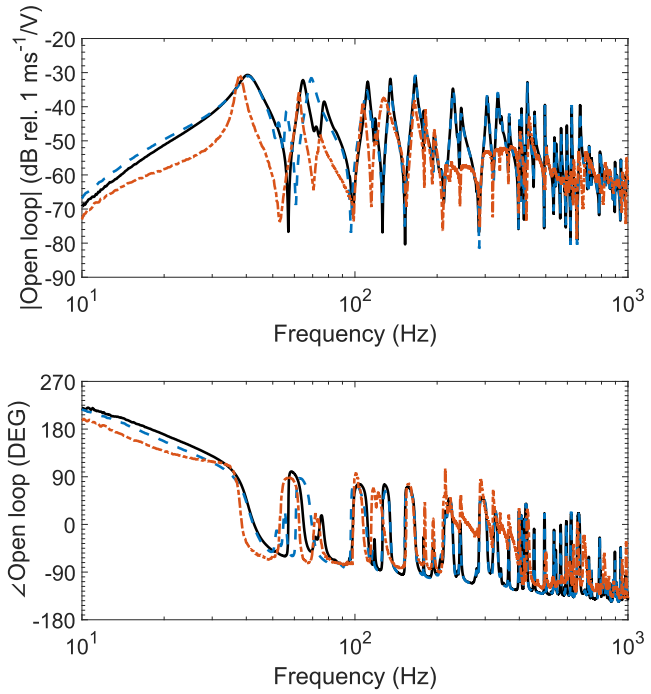

Fig. 2. Bode plots of the open loop sensor-actuator frequency response functions for the voltage-driven actuators. Classical configuration (solid black line), the classical configuration with the same proof mass as that of the flywheel configuration (dashed blue line), and with the flywheel proof actuator (dash-dotted red line)

Considering the proof mass actuators shown in Fig. 2, the modulus plot is characterized by a heavily damped resonance peak at the fundamental resonance of the proof mass actuator and then a sequence of rounded resonance peaks and antiresonance lows pairs. The phase plot is characterized by a -180° phase lag at the fundamental resonance frequency of the actuator and then a sequence of -180° phase lag and $+180^\circ$ phase lead for each resonance peak and antiresonance low pair of the plate.

The plot shows that the axial inertia effect produced by the flywheel element shifts the resonance peak at the fundamental resonance of the proof mass actuator to a lower frequency.

The stability of the velocity feedback loops using the classical configuration, classical with the same proof mass as the flywheel configuration and the flywheel proof mass actuator is assessed using the Nyquist criterion presented in Fig. 3. The Nyquist diagram for the open loop sensor-actuator frequency response function for the voltage-driven classical proof mass actuator shown with solid black line is characterized by a circle in the real negative quadrants, which is linked to the resonance effect generated by the fundamental resonance effect of the actuator. While the series of progressively smaller circles in the real positive quadrants are linked to the resonance effects produced by the flexural natural modes of the plate. The circle in the left-hand quadrants indicates that the feedback loop is only conditionally stable with a maximum signal gain margin of about 54 dB.

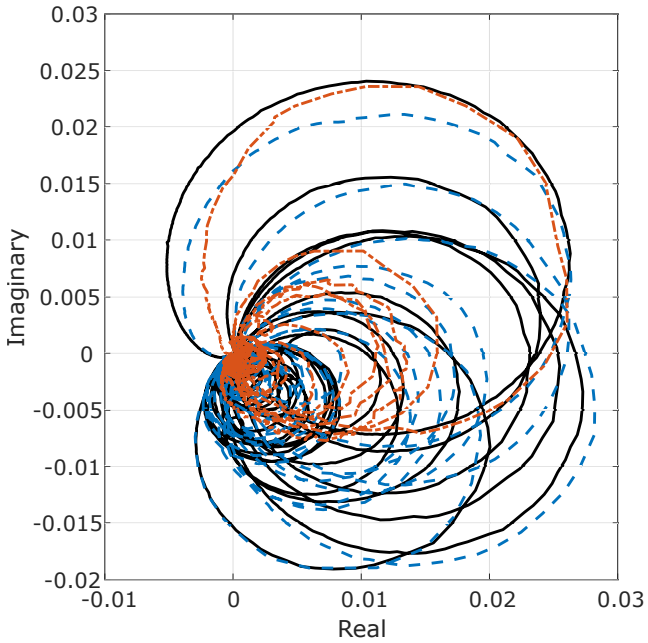

Fig. 3. Nyquist diagram for the open loop sensor-actuator frequency response function for the voltage-driven proof mass actuators. Classical configuration (solid black line), the classical configuration with the same proof mass as that of the flywheel configuration (dashed blue line), and with the flywheel proof actuator (dash-dotted red line)

The Nyquist plot for the classical actuator with the same proof mass as the flywheel configuration shown with the dashed blue line presents similar characteristics to the classical configuration. The circle in the left-hand quadrants indicates that the stability gain margin is about 55 dB. Finally, analyzing the Nyquist plot for the flywheel-proof mass actuator shown with a dashed black line the circle in the left-hand quadrants indicates that the stability gain margin is about 68 dB.

4. PERFORMANCE

The control performance of the velocity feedback loops with the three configurations of the proof mass actuator is assessed on a thin rectangular plate shown in Fig. 4. The proof mass actuator is attached on one side of the plate with an M5 nut which was glued to the structure, while the ICP 352C65 accelerometer is attached with wax on the opposite side at transducer footprint. The accelerometer is power supplied using a 480B10 sensor signal conditioner. The integrated signal is sent to the actuator through the QD4480 liner amplifier. The clamped thin rectangular plate is excited with a stochastic vibration generated with the point force shaker. The shaker was attached to

the base structure and attached to the plate using a stinger and via a 288D1 force sensor. The mechanical properties of the steel plate and the coordinates of the actuator and shaker are reported in Table 2. To keep the focus on the analysis of the flywheel proof mass actuators, only a simple fixed gain controller was implemented.

Fig. 4. Picture of the test setup used to assess the control performance of the closed loop sensor-actuator for the voltage-driven proof mass actuators

Table 2
Mechanical parameters of the steel panel

Parameter	Value
Length	668 mm
Width	444 mm
Thickness	1.4 mm
Density	8200 kg/m^3
Elastic modulus	210 GPa
Poisson ratio	0.31
Damping ratio	0.0035
Actuator coordinate	(234, 178) mm
Shaker coordinate	(433, 157) mm

4.1. Performance at the control position

The control performance of the velocity feedback loops with the classical configuration, the classical configuration with the same proof mass as that of the flywheel configuration, and the flywheel proof mass configuration are first assessed by plotting the velocity of the rectangular plate at the control position. Figure 5 shows the control performance of the velocity feedback loops implemented with maximum signal gains that ensure stability. The control velocity signal per unit force of excitation is considered for the plane plate (dotted green line) and the plate with the velocity feedback loop using the classical actuator (solid black line), the classical actuator with the same proof mass as the flywheel configuration (dashed blue line) and the flywheel proof mass actuator (dashed-dotted red line).

Considering first the spectrum of the plane rectangular plate, the flexural response at the control position is characterized by a sequence of progressively smaller amplitude sharp resonance peaks. When the velocity feedback loops are implemented with

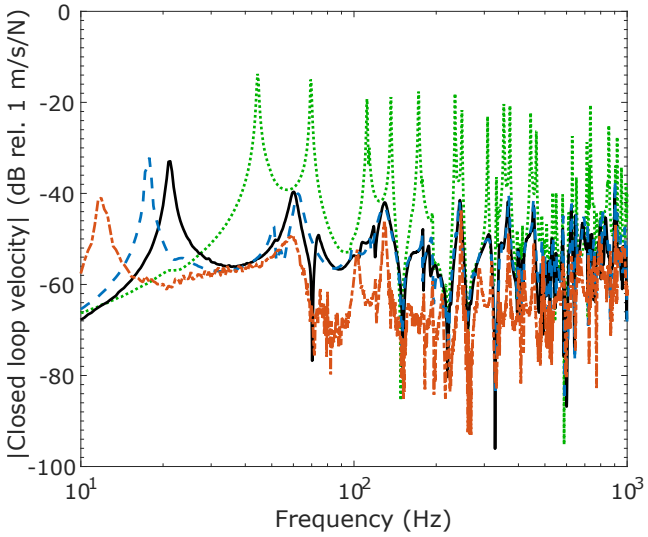

Fig. 5. Closed loop sensor-actuator frequency response function per unit force excitation at the control position for the voltage-driven proof mass actuators. Plane plate (dotted green line), classical configuration (solid black line), the classical configuration with the same proof mass as that of the flywheel configuration (dashed blue line), and with the flywheel proof actuator (dash-dotted red line)

maximum control gains that ensure stability using the proof mass actuators, the response at the control position is characterized by rounded-off plate resonance peaks. However, the velocity feedback loops also generate a high control spillover effect at the fundamental resonance frequency of the proof mass actuators. The sharp peaks caused by the spillover effect increase with increasing signal gain applied to the proof mass actuators implemented in the velocity feedback loops. Thus, for the classical configuration of the proof mass actuator, the spillover appears at about 20 Hz, for the classical configuration with the same proof mass as that of the flywheel configuration at about 18 Hz, while for the pinned flywheel proof mass actuator at about 12 Hz. What is worth noticing, the spillover effect produced by the flywheel configuration has a lower amplitude of about 8 dB compared to the other two configurations. Also, at higher frequencies, the control performance of the flywheel configuration is much greater compared to the other two configurations.

Figure 6 presents the control performance of the velocity feedback control loops analyzed with 10 Hz to 1 kHz frequency-averaged closed-loop sensor-actuator frequency response functions per unit force excitation with reference to increasingly higher feedback control gains. The reductions are normalized with reference to the frequency-averaged plain rectangular plate. The results show the frequency-averaged plate reduction with increasing feedback control gains up to maximum control gain that guarantees stability for the feedback loops implemented with proof mass actuators considered in this study.

The analysis of results for the classical configuration shows that the feedback control loop produces up to 11.4 dB reduction of the velocity reductions at the control position with a maximum control gain of 54 dB. The performance of the velocity

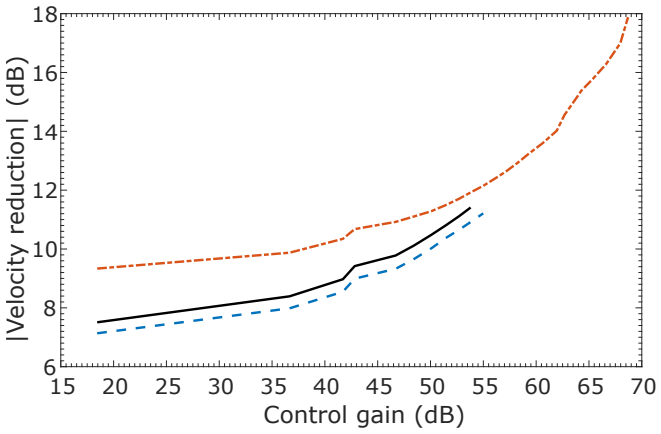

Fig. 6. Control velocity reductions of the frequency-averaged closed-loop sensor-actuator frequency response functions. Classical configuration (solid black line), the classical configuration with the same proof mass as that of the flywheel configuration (dashed blue line), and with the flywheel proof mass actuator (dash-dotted red line)

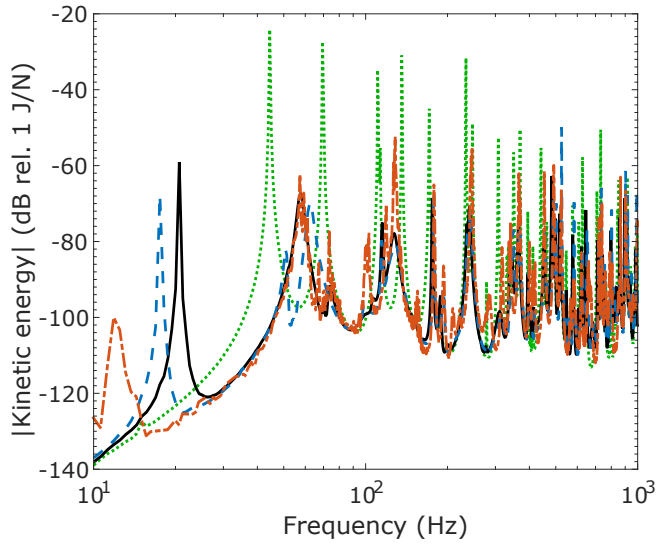

Fig. 7. Total flexural kinetic energy per unit force excitation of the plate with maximum signal gain. Plane plate (dotted green line), classical configuration (solid black line), the classical configuration with the same proof mass as that of the flywheel configuration (dashed blue line), and with the flywheel proof actuator (dash-dotted red line)

feedback loop is slightly lower when the classical configuration that has the same proof mass as that of the flywheel configuration is used. The results presented with the dashed blue line show that the velocity feedback loop can generate only up to 11.3 dB reduction with a maximum control gain of 55 dB. Finally, the feedback loop with the flywheel proof actuator shown with a dashed-dotted red line can implement much larger feedback control gains of up to 59 dB such that the frequency-averaged velocity of the plate is reduced by up to 17.9 dB. The improved control performance by about 6.5 dB compared to the classical configuration and by about 6.6 dB compared to the classical configuration that has the same proof mass as that of the flywheel configuration is obtained thanks to the possibility of implementing much higher stable control gains.

4.2. Overall performance

The performance of the feedback loops with the compared proof mass actuators was assessed considering the total flexural kinetic energy of the thin rectangular plate. Figure 7 shows spectra of the total flexural kinetic energy of the panel per unit force excitation for the plate without actuators and when the velocity feedback loop using the three proof mass actuators is implemented with maximum control gains that ensure stability. Figure 7 shows results for the plain plate (dotted green lines) and for the plate with the classical proof mass actuator (solid black line), with the classical configuration with the same proof mass as that of the flywheel configuration (dashed blue line) and with flywheel proof mass actuator (dashed-dotted red line). The plate flexural kinetic energy per unit force excitation effects presented in Fig. 7 were derived when the velocity feedback loops are implemented with maximum control gains that ensure stability.

The spectrum of the kinetic energy per unit force excitation for the plain plate is characterized by a sharp resonance peak at about 44 Hz, which is due to the fundamental natural mode of the plate and a sequence of sharp resonance peaks progressively smaller in amplitude due to flexural modes of the plate. When the feedback loop with the proof mass actuators is implemented with maximum control gains that ensure stability, the spectra of the kinetic energy are characterized by rounded-off plate resonance peaks.

The first two resonance peaks are rounded-off by about 81 dB and by about 58 dB. The results show that all three velocity feedback loops produce similar vibration control performance in the entire frequency band. The measured and simulated spectra of the kinetic energy also show the pinning effect of the plate at about 60 Hz and about 130 Hz.

The measured spectra also show that the velocity feedback loops with proof mass actuators generate high control spillover effect in correspondence to the fundamental resonance frequency of the actuators. However, the feedback loops using the flywheel proof actuator produce a much smaller control spillover effect. This is because when the actuators are equipped with the flywheel, the spillover occurs at a much lower frequency in correspondence to the fundamental resonance. Thus, when the feedback loop with the flywheel proof actuator is implemented the spillover effect is about 40 dB lower compared to the classical configuration and about 30 dB lower compared to the classical configuration with the same proof mass as the flywheel actuator. It can be noticed that the measured performance of the velocity feedback loops with the flywheel proof mass actuator is slightly more disturbed at lower frequencies compared to the other two configurations, most probably due to additional rotational oscillations of the flywheel element itself.

Figure 8 presents the frequency-averaged plate kinetic energy reduction with reference to increasingly higher feedback control gains. The reductions are normalized with reference to the frequency-averaged plate kinetic energy of the plain rectangular plate. The results show the frequency-averaged plate kinetic energy reduction with increasing feedback control gains

up to maximum control gain that guarantees stability for the feedback loops implemented with proof mass actuators considered in this study.

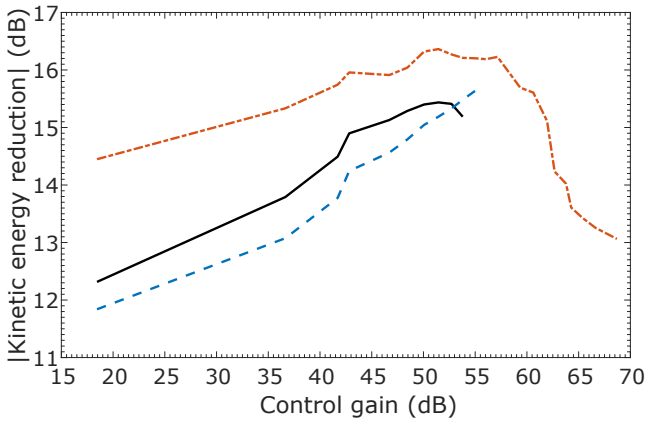

Fig. 8. Reductions of the 10 Hz – 1 kHz frequency-averaged kinetic energy produced by the feedback loops. Classical configuration (solid black line), the classical configuration with the same proof mass as that of the flywheel configuration (dashed blue line), and with the flywheel proof actuator (dash-dotted red line)

The feedback loop with classical proof mass actuator shown with a solid black line produces up to 15.4 dB reduction of the frequency-averaged kinetic energy with a maximum control gain of 54 dB. The feedback loops with the classical configuration that has the same proof mass as the flywheel configurations shown with a dashed blue line produce up to 15.6 dB reduction with a maximum control gain of 55 dB. When the flywheel proof mass actuator, shown with a dashed dotted red line is used, it can implement much larger feedback control gains of up to 68 dB, and the frequency-averaged kinetic energy of the plate is reduced by up to 16.4 dB.

The drop in the frequency-averaged kinetic energy performance of the control system is caused by high signal gains applied to the control actuator, which instead of reducing vibrations create a pinning effect of the plate presented and described in Fig. 7. Nevertheless, the presented experimental results show that improved control performance of the velocity feedback loops with flywheel proof mass actuator is obtained thanks to the possibility of implementing much higher control gains.

5. CONCLUSIONS

This paper presents a new proof mass electromagnetic actuator with a flywheel element that can be effectively used in velocity feedback control loops to reduce the flexural vibrations of a thin rectangular panel. Three different configurations of the proof actuator were considered and compared with each other. The stability and control performance of velocity feedback loops were considered using a classical proof actuator, a classical actuator with the same proof mass as that of the flywheel configuration, and a flywheel proof actuator. Experimental test results carried out on a test rig with a thin rectangular panel were compared using three proof mass actuators.

The stability analysis shows that the addition of the flywheel element increases the gain margin of the feedback loops. Moreover, compared to the classical configuration with the same proof mass as that of the flywheel configuration, the flywheel prototype increased the gain margin without any increase in the actuator weight.

The performance analysis shows that the addition of the flywheel element in a proof mass actuator can increase the performance of the velocity feedback loops, both at the control position and its overall effectiveness at a thin rectangular panel thanks to the possibility of implementing much higher stable control gains.

The experimental results presented in this paper confirmed that the flywheel proof mass actuators can improve stability and control performance of the velocity feedback loops to reduce the broadband vibration of a thin plate. The improved control performance was obtained thanks to the lower fundamental resonance frequency of the proof mass actuator and thus the possibility to implement much higher control signal gain.

The proposed design would be beneficial in any type of transportation vehicle where there are irregular dynamics of the motion, which cause high accelerations or shocks, for example, planes when landing, and underground trains going through tunnels.

ACKNOWLEDGEMENTS

The authors gratefully acknowledge the European Commission for its support of the Marie Skłodowska-Curie program through the ITN ANTARES project (GA 606817).

REFERENCES

[1] C.G. Diaz and P. Gardonio, "Feedback control laws for proof-mass electro-dynamic actuators," *J. Smart Mater. Struct.*, vol. 16, pp. 1766–83, 2007.

[2] C.G. Diaz, C. Paulitsch, and P. Gardonio, "Smart panel with active damping units. Implementation of decentralized control," *J. Acoust. Soc. Am.*, vol. 124, pp. 898–910, 2008.

[3] M. Balas, "Direct velocity feedback control of large space structures," *J. Guid. Control Dyn.*, vol. 2, no. 3, pp. 252–253, 1979.

[4] D.W. Miller and E.F. Crawley, "Theoretical and experimental investigation of space-realizable inertial actuation for passive and active structural control," *J. Guid. Control Dyn.*, vol. 11, no. 5, pp. 449–458, 1988.

[5] F. Fahy and P. Gardonio, *Sound and structural vibration. Radiation, Transmission and Response, 2nd ed.*, Academic Press, Oxford, 2007.

[6] H. Politansky and W.D. Pilkey, "Suboptimal feedback vibration control of a beam with a proof-mass actuators," *J. Guid. Control Dyn.*, vol. 12, pp. 691–697, 1989.

[7] D.C. Zimmerman and D.J. Inman, "On the nature of the interaction between structures and proof mass actuators," *J. Guid. Control Dyn.*, vol. 13, no. 1, pp. 82–88, 1990.

[8] A. Preumont, *Vibration Control of Active Structures*, Kluwer Academic, Dordrecht, 2002.

[9] C. Paulitsch, *Vibration control with electrodynamic actuators*, VDI Verlag, Düsseldorf, 2005.

[10] A. Kras and P. Gardonio, "Active vibration control unit with a flywheel inertial actuator," *J. Sound Vib.*, vol. 464, p. 114987, 2020.

[11] A. Preumont, *Mechatronic dynamics of electromechanical and piezoelectric systems*, Springer, Dordrecht, 2006.

[12] C. Paulitsch, P. Gardonio, S.J. Elliott, P. Sas, and R. Boonen, "Design of a lightweight, electrodynamic, inertial actuator with integrated velocity sensor for active vibration control of a thin lightly-damped panel," *Proc. of the ISMA 2004 Int. Conf. Leuven*, 2004, pp. 239–53.

[13] G. Parmar, D.B. Hiemstra, Y. Chen, and S. Awtar, "A moving magnet actuator for large range nanopositioning," *Proceedings of the ASME Conference*, 2001, pp. 41–48.

[14] S. Cinquemani, G. Cazzulani, A. Costa, and F. Resta, "Design of a stand-alone active damper for distributed control of vibration," *Proc. SPIE 9799 Active and Passive Smart Structures and Integrated Systems*, pp. 1–8, 2016.

[15] D.K. Lindner, T.P. Celano, and E.N. Ide, "Vibration suppression using a proofmass actuator operating in stroke/force saturation," *J. Vib. Acoust.*, vol. 113, pp. 423–33, 1991.

[16] D.K. Lindner, G.A. Zvonar, and D. Borojevic, "Performance and control of proof-mass actuators accounting for stroke saturation," *J. Guid. Control Dyn.*, vol. 17, no. 5, pp. 1103–1108, 1994.

[17] N. Alujević, H. Wolf, P. Gardonio, and I. Tomac, "Stability and performance limits for active vibration isolation using blended velocity feedback," *J. Sound Vib.*, vol. 330, no. 21, pp. 4981–4997, 2011.

[18] L. Benassi and S.J. Elliott, "Active vibration isolation using an inertial actuator with local displacement feedback control," *J. Sound Vib.*, vol. 278, no. 4-5, pp. 705–724, 2004.

[19] L. Benassi, S.J. Elliott, and P. Gardonio, "Active vibration isolation using an inertial actuator with local force feedback control," *J. Sound Vib.*, vol. 276, no. 1–2, pp. 157–179, 2004.

[20] J. Rohlfing, P. Gardonio, and S.J. Elliott, "Feedback compensator for control units with proof-mass electrodynamic actuators," *J. Sound Vib.*, vol. 331, no. 15, pp. 3437–3450, 2012.

[21] M.D. Borgo, M.G. Tehrani, and S.J. Elliott, "Nonlinear control and stability analysis of a stroke limited inertial actuator in velocity feedback," *Proc. of the 9th European Nonlinear Dynamics Conference ENOC*, 2017, pp. 1–10.

[22] M.C. Smith, "Synthesis of mechanical networks: the inerter," *IEEE Trans. Autom. Control*, vol. 47, no. 10, pp. 1648–1662, 2002.

[23] P. Brzeski, M. Lazarek, and P. Perlikowski, "Experimental study of the novel tuned mass damper with inerter which enables changes of inertance," *J. Sound Vib.*, vol. 404, pp. 47–57, 2017.

[24] A. Kras and P. Gardonio, "Velocity feedback control with a flywheel proof mass actuator," *J. Sound Vib.*, vol. 402, pp. 31–50, 2017.

[25] N. Alujević, D. Čakmak, H. Wolf, and M. Jokić, "Passive and active vibration isolation systems using inerter," *J. Sound Vib.*, vol. 418 pp.163–183, 2018.

[26] M. Zilletti, "Feedback control unit with an inerter proof-mass electrodynamic actuator," *J. Sound Vib.*, vol. 369, pp. 16–28, 2016.